

**Coexistence of induced superconductivity and quantum Hall states in InSb nanosheets**Jinhua Zhi,<sup>1</sup> Ning Kang,<sup>1,\*</sup> Feifan Su,<sup>2</sup> Dingxun Fan,<sup>1</sup> Sen Li,<sup>1</sup> Dong Pan,<sup>3</sup> S. P. Zhao,<sup>2</sup> Jianhua Zhao,<sup>3,†</sup> and H. Q. Xu<sup>1,4,‡</sup><sup>1</sup>*Beijing Key Laboratory of Quantum Devices, Key Laboratory for the Physics and Chemistry of Nanodevices and Department of Electronics, Peking University, Beijing 100871, China*<sup>2</sup>*Beijing National Laboratory for Condensed Matter Physics, Institute of Physics, Chinese Academy of Sciences, Beijing 100190, China*<sup>3</sup>*State Key Laboratory of Superlattices and Microstructures, Institute of Semiconductors, Chinese Academy of Sciences, P.O. Box 912, Beijing 100083, China*<sup>4</sup>*Beijing Academy of Quantum Information Sciences, Beijing 100193, China*

(Received 30 October 2018; revised manuscript received 19 May 2019; published 14 June 2019)

Hybrid superconducting devices based on high-mobility two-dimensional electron gases with strong spin-orbit coupling are considered to offer a flexible and scalable platform for topological quantum computation. Here, we report the realization and electrical characterization of hybrid devices based on high-quality InSb nanosheets and superconducting niobium (Nb) electrodes. In these hybrid devices, we observe gate-tunable proximity-induced supercurrent and multiple Andreev reflections, indicating a transparent Nb-InSb nanosheet interface. The high critical magnetic field of Nb combined with high-mobility InSb nanosheets allows us to exploit the transport properties in the exotic regime where the superconducting proximity effect coexists with the quantum Hall effect. Transport spectroscopy measurements in such a regime reveal an enhancement of the conductance at the quantum Hall plateaus, accompanied by a pronounced zero-bias peak in the differential conductance. We discuss that these features originate from the formation of Andreev edge states at the superconductor-InSb nanosheet interface in the quantum Hall regime. In addition to shedding light on the interplay between superconductivity and quantum Hall effect, our work opens a new possibility to develop hybrid superconducting devices based on 2D semiconductor nanosheets with strong spin-orbit coupling.

DOI: [10.1103/PhysRevB.99.245302](https://doi.org/10.1103/PhysRevB.99.245302)**I. INTRODUCTION**

In recent years, two-dimensional (2D) III-V compound semiconductors have attracted great attention due to their unique charge-transport properties and potential applications in electronics and optoelectronics [1–3]. Among them, InSb provides an ideal experimental platform for quantum transport studies owing to its high mobility, small effective carrier mass, narrow band gap, and strong spin-orbit interaction [4–7]. In particular, a prominent feature resulting from the combination of superconductor and strong spin-orbit interaction in low-dimensional InSb materials is the formation of topological superconducting channels, hosting Majorana bound states (MBSs) in solid-state devices [8,9]. Recent experiments performed on hybrid devices based on InSb nanowires coupled to superconductors have shown the zero-bias conductance peaks as a signature of the zero-energy MBSs [10–13]. More recently, there is growing interest in hybrid superconducting devices based on high-mobility two-dimensional electron gas (2DEG) with strong spin-orbit interaction, which can offer a flexible platform for topological quantum computation in a scalable way [14–17].

In the presence of a strong perpendicular magnetic field, the orbital motion of electrons in 2DEG is quantized with the formation of Landau levels, giving rise to the quantum

Hall effect (QHE). Recent theoretical and experimental developments have explored the hybrid superconducting systems beyond the traditional low-magnetic-field regime for understanding the interplay between superconductivity and QHE in 2DEG [18–25]. An interesting feature is that the phase-coherent Andreev reflections and the flow of supercurrent in chiral edge channels are distinct from that offered by conventional charge transport at normal conductor-superconductor interfaces under zero field. Many intriguing quantum phenomena arise due to the induced superconducting correlation at the 2DEG-superconductor interface in the quantum Hall regime, such as Andreev edge states [26–32], non-Abelian zero modes [21–24], and crossed Andreev conversion [20,33,34]. In practice, experimental access to such a coexistence of superconductivity and quantum Hall states requires both a high-quality 2D system with a low-magnetic-field onset of the QHE and superconducting contacts with high upper critical field. Recently, induced superconducting correlation and supercurrent in the quantum Hall regime have been demonstrated in high-mobility graphene-based hybrid devices [18–20]. However, it still remains a challenging task to achieve the coexistence of the superconducting proximity effect and quantum Hall effect in semiconducting 2DEG with strong spin-orbit interaction and a desired high carrier mobility. Due to the formation of Schottky barriers at the metal-semiconductor interfaces, the achievement of transparent superconductor-2DEG interfaces is a prime challenge. Very recently, we have succeeded in growing freestanding high-quality two-dimensional InSb nanosheet by means of molecular-beam epitaxy (MBE) [35]. Electrical characterization shows that these InSb nanosheets

\*Corresponding author: [nkang@pku.edu.cn](mailto:nkang@pku.edu.cn)†Corresponding author: [jhzhao@red.semi.ac.cn](mailto:jhzhao@red.semi.ac.cn)‡Corresponding author: [hqxu@pku.edu.cn](mailto:hqxu@pku.edu.cn)

exhibit a high electron mobility at low temperature. In contrast to conventional InSb quantum well heterostructures using thick buffer layers [36,37], these single-crystalline InSb layers offer a suitable platform to fabricate high-quality hybrid devices, enabling efficient gate-voltage tunability and direct low-resistance contacts without a postdeposition annealing, which may induce the defect states and surface leakage.

In this work, we report the realization of hybrid superconducting devices based on high-quality InSb nanosheets with superconducting electrodes made of niobium (Nb). We demonstrate that the hybrid devices show a gate-tunable superconducting proximity effect and multiple Andreev reflections, indicating transparent superconductor-InSb nanosheet interfaces. Taking advantage of the high mobility of the InSb nanosheet and the high critical field of Nb, we access the regime where the superconducting proximity effect coexists with the quantum Hall effect. In such a regime, transport measurements reveal an enhancement of conductance at the quantum Hall plateaus, accompanied by a pronounced zero-bias peak in the differential conductance. We attribute these results to the formation of Andreev edge states at the superconductor-InSb nanosheet interfaces in the quantum Hall regime. Our results may pave the way for developing complex and controllable topological devices based on high-mobility two-dimensional electron gas with strong spin-orbit coupling.

## II. EXPERIMENTAL DETAILS

InSb nanosheets used in this work were grown by MBE with pure zinc-blende crystal structure. The left panel of Fig. 1(a) shows a scanning electron microscope (SEM) image of an as-grown freestanding InAs nanowire/InSb nanosheet heterostructure on a *p*-type Si(111) substrate. The right panel of Fig. 1(a) is a high-resolution transmission electron microscope (TEM) image of the side section of the InSb nanosheet, exhibiting a high-quality crystal structure. The thicknesses of the InSb nanosheets range from 10 to 80 nm, with lengths of 2–10  $\mu\text{m}$  and widths of 500 nm to 2  $\mu\text{m}$ . Subsequent to the growth, the nanosheets were mechanically transferred onto a degenerately doped, *n*-type Si substrate (used as a global back gate) covered with a 200-nm-thick thermal oxide. Electrodes were patterned with standard electron-beam lithography using a bilayer of polymethyl methacrylate (PMMA) 950 K A4 and MMA EL9 resists. Nb (100 nm) was deposited by magnetron sputtering after a diluted  $[(\text{NH}_4)_2\text{S}_x]$  solution etching. An SEM image of a representative Josephson junction based on an InSb nanosheet is displayed in the insert of Fig. 1(c). The length  $L$  between the source and drain electrodes was varied from 150 to 250 nm and the junction width  $W$  of 3–5  $\mu\text{m}$ . Nb test strips of 50  $\mu\text{m}$  in length and 300 nm to 1  $\mu\text{m}$  in width were deposited with the same parameters of the electrodes. The superconducting critical temperature of the test strips was determined to be  $T_c = 7.2$  K (see Supplemental Material, Fig. S1 [38]), a bit below the critical temperature of bulk niobium (9.25 K). Applying a magnetic field oriented perpendicular to the film plane, the upper critical magnetic field at 2.0 K was determined to be  $H_{c2} = 6$  T. The critical magnetic field increased slightly upon lowering the temperature from 2.0 K down to base temperature and decreased when the width of the test strip dropped from 1  $\mu\text{m}$  to 300 nm. The

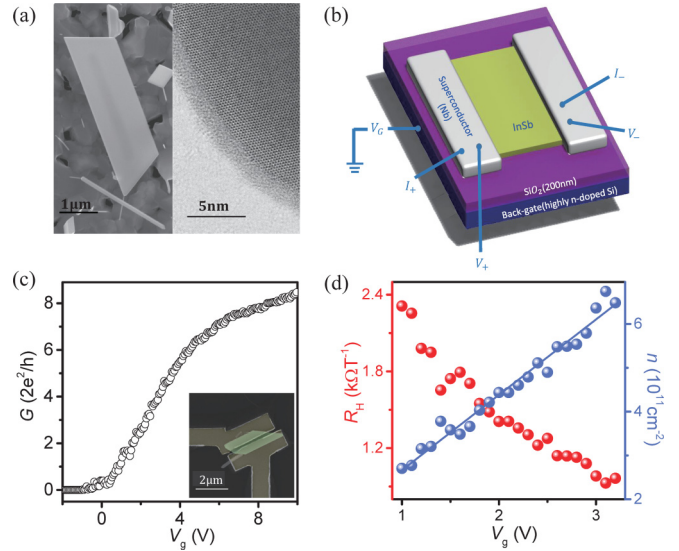


FIG. 1. Characterization of InSb nanosheets. (a) SEM and TEM images of synthesized InSb nanosheets. The 2D InSb nanosheets were epitaxially grown on freestanding 1D InAs nanowires on a *p*-type Si(111) substrate. (b) Schematic of the Josephson junction geometry based on InSb nanosheet with global back gate and the measurement setup. (c) Two-terminal conductance vs gate voltage  $V_g$ . Data taken at  $V_{\text{bias}} = 1$  mV and  $T = 60$  mK. From the transfer characteristics of the device, we can extract a field-effect electron mobility of  $\mu \simeq 6000$   $\text{cm}^2 \text{V}^{-1} \text{s}^{-1}$ . Inset: false-color SEM image of a fabricated Nb-InSb nanosheet hybrid device: brown–Nb contact, green–InSb nanosheet. (d) Low-field Hall coefficients  $R_H$  (red dots) and carrier densities  $n$  (blue dots) as a function of the back-gate voltage  $V_g$ . The blue line is a linear fit to the  $n - V_g$  data.

transport measurements were carried out using four-terminal dc/ac (standard lock-in techniques) schemes, as shown in Fig. 1(b).

## III. RESULTS AND DISCUSSION

### A. InSb nanosheet characteristics

Figure 1(c) shows the two-probe conductance of an InSb nanosheet device with Ti/Au (5/90 nm) electrodes as a function of the back-gate voltage  $V_g$  taken at  $T = 60$  mK. The device displays stable and well-reproduced transfer characteristics at low temperatures, indicating a good surface quality of the InSb nanosheet (see Supplemental Material, Fig. S2 [38]). From the transfer characteristic curve, we can estimate that the field-effect electron mobility  $\mu$  is about  $6000$   $\text{cm}^2 \text{V}^{-1} \text{s}^{-1}$ . Figure 1(d) displays the measurements on an InSb nanosheet device with Hall-bar configuration taken at  $T = 60$  mK. Carrier density  $n$  is extracted from gate-dependent Hall coefficient and increases linearly from  $\sim 2.7 \times 10^{11}$  to  $\sim 6.7 \times 10^{11}$   $\text{cm}^{-2}$  with  $V_g$  increases from 1 to 3.2 V. With the same fabrication and measurement process, the electron mobility up to  $\sim 18000$   $\text{cm}^2 \text{V}^{-1} \text{s}^{-1}$  in InSb nanosheet devices was reported in our previous work [35]. Such a high electron mobility at low carrier densities makes it possible to observe the quantum Hall state of a small filling factor at a relatively low magnetic field.

### B. Proximity-induced superconductivity in the two-dimensional InSb nanosheets

Having identified the high quality of the MBE-grown InSb nanosheets, we can now investigate transport through Josephson junctions and characterize the transparency of the Nb-InSb nanosheet interface, which is one of the key parameters for hybrid superconducting devices. Figure 2(a) shows the voltage-current ( $V_{sd} - I_{\text{bias}}$ ) characteristics of the Nb-InSb nanosheet-Nb hybrid device at different gate voltages  $V_g$  and base temperature  $T = 10$  mK. The current flowing with no voltage drop below the critical current  $I_c$  is observed, which gives a direct evidence of the proximity-induced superconductivity in the superconductor-InSb nanosheet Josephson junction. Beyond  $I_c$ , a finite source-drain voltage drop abruptly appears, signifying the switch from the superconducting state to the dissipative resistive state. To give more details about the dependence of the supercurrent on  $V_g$ , we plot the differential resistance  $dV_{sd}/dI_{\text{bias}}$  versus the applied gate voltage  $V_g$  and bias current  $I_{\text{bias}}$ , as shown in Fig. 2(b). The central dark region corresponding to the zero-resistance supercurrent branch is separated from the red region which contains dissipative quasiparticle tunneling by the bright lines (where  $I_c$  is defined). It can be clearly seen that the magnitude of  $I_c$  is gate-voltage dependent and can be tuned from 0 to 25 nA while  $V_g$  varies from 1.5 to 12 V. Meanwhile,  $I_c$  exhibits repro-

ducible and time-independent fluctuations which we attribute to phase-coherent diffusive motion of carriers in a disordered junction device.

Figure 2(c) shows the differential conductance  $dI_{sd}/dV_{\text{bias}}$  as a function of source-drain bias voltage  $V_{\text{bias}}$ . The induced superconductivity manifests itself also in the form of a subharmonic gap structure at finite bias due to multiple Andreev reflections. In a multiple-Andreev-reflections process, an electron (hole) from the N region is reflected at the N-S interface as a phase-conjugated hole (electron), and between two reflections, the electron (hole) gains an energy of  $eV_{\text{bias}}$ . This happens several times until the energy of the electron (hole) is above the superconducting energy gap. The subgap structure consists of a series of conductance peaks at source-drain voltages  $V_{\text{bias}} = 2\Delta/en$  ( $n = 1, 2, \dots$ ), which enables us to determine the superconducting gap,  $\Delta$ . The conductance peak corresponding to  $n = 1$  is located at  $V_{\text{bias}} = 2\Delta/e = 2.4$  mV, from which we can evaluate the superconducting gap,  $\Delta = 1.2$  meV, comparable to previous measurements on Nb-InSb nanowire hybrid devices [10–13]. Employing the electron-phonon coupling strength  $2\Delta = 3.9k_B T_c$  and adopting  $\Delta = 1.2$  meV as the zero-temperature superconducting gap, a critical temperature  $T_c \approx 7.2$  K for the Nb electrodes is derived, which coincides with the measured value of  $T_c$  (see Supplemental Material, Fig. S1 [38]). The Andreev reflection at the S-N interface, which can be viewed as one of the microscopic origins of the proximity effect, requires a transparent interface.

The transparent N-S interface of our devices can be also certified by the derived transmission coefficient from the  $I_{sd} - V_{\text{bias}}$  curves. In the Blonder-Tinkham-Klapwijk (BTK) theory for Andreev reflection [42,43], the strength of the potential barrier at a N-S interface can be characterized by a parameter  $Z$ .  $Z$  is a dimensionless scattering parameter and is usually extracted from the ratio  $eI_{\text{exc}}R_n/\Delta$  (here  $R_n$  is the normal state resistance and  $I_{\text{exc}}$  is the excess current).  $I_{\text{exc}}$  is the nonzero current offset at  $V_{\text{bias}} = 0$  obtained by the linear extrapolation of the current-voltage characteristics at  $V_{\text{bias}} > 2\Delta/e$ , and  $R_n$  can be derived from the linear fit to the measured current-voltage curve at  $V_{\text{bias}} > 2\Delta/e$ . An  $I_{sd} - V_{\text{bias}}$  curve of the junction measured at gate voltage  $V_g = 1$  V is shown in Fig. 2(d). Using the extracted superconducting gap  $\Delta = 1.2$  meV, we obtain  $Z \sim 0.88$ . The inset in Fig. 2(d) shows a typical evolution of the transmission coefficient  $Tr = 1/(1 + Z^2)$  as a function of gate voltage. Then we can evaluate the average value of the transmission coefficient  $Tr \sim 0.6$  (see Supplemental Material, Fig. S3 for more details [38]). This transmission coefficient means that about 60 percent of the injected electrons perform Andreev reflection and insures that the signal originating from Andreev reflection is not buried in normal scattering. For our Nb-InSb nanosheet device junction, we also obtain  $I_c R_n \approx 75 \mu\text{V}$  at low temperatures (see Supplemental Material, Fig. S3 [38]). This value is significantly smaller than the BCS superconducting gap of bulk Nb. Such suppression of the  $I_c R_n$  product has been commonly observed in superconductor-nanostructure weak links and has been attributed to the effects of premature switching and a reduced superconducting gap at the interface [44,45].

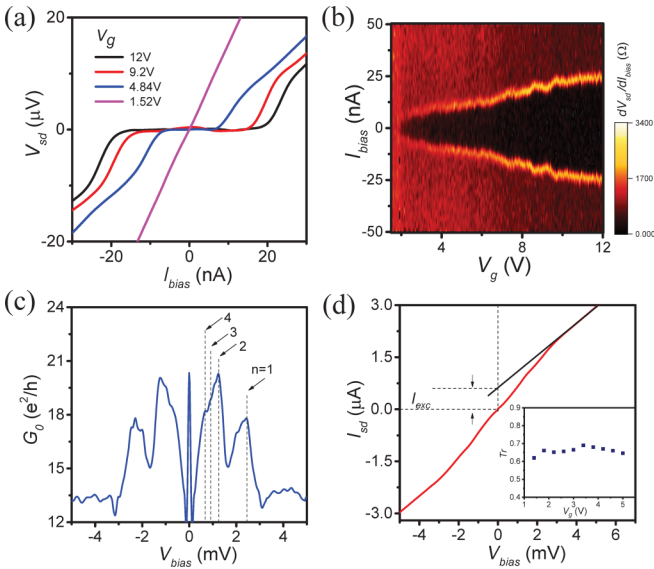


FIG. 2. Gate-modulated supercurrent in an InSb nanosheet Josephson junction. (a)  $V_{sd} - I_{\text{bias}}$  characteristics at  $T = 10$  mK and various back gate voltages  $V_g$  showing the modulation of the critical current. (b) Color-scale plot of differential resistance  $dV_{sd}/dI_{\text{bias}}$  vs  $V_g$  and  $I_{\text{bias}}$  at  $T = 10$  mK and  $B = 0$  T. (c) Differential conductance  $dI_{sd}/dV_{\text{bias}}$  vs  $V_{\text{bias}}$  measured at  $V_g = 1$  V and  $T = 10$  mK. The arrows and vertical dotted lines indicate conductance peaks at voltage positions  $eV_n = 2\Delta/n$  ( $n = 1, 2, 3, \dots$ ), corresponding to multiple Andreev reflections. (d) Current-voltage characteristics with the same condition as in (c). The linear fit of the current-voltage curve at  $V_{\text{bias}} > 2\Delta/e$  extends to a finite value of the current at zero-bias voltage, i.e., excess current  $I_{\text{exc}}$ . The inset shows a typical evolution of the transmission coefficient as a function of gate voltage.

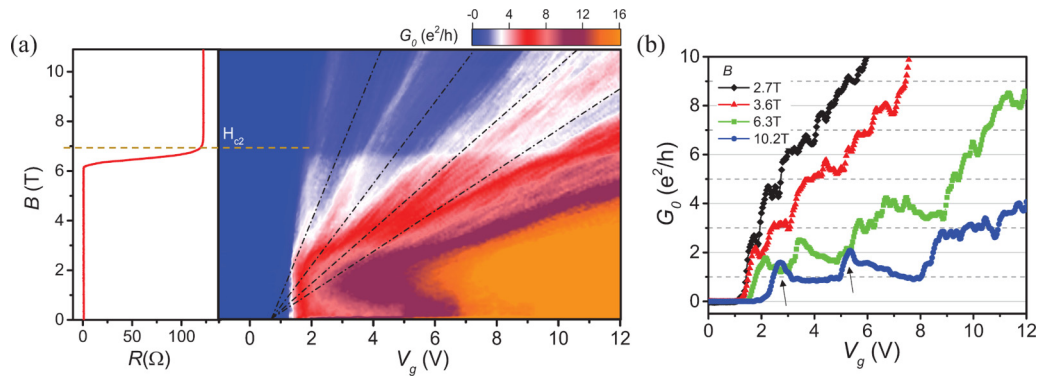


FIG. 3. The coexistence of superconductivity and quantum Hall states. (a) Right panel: color-scale plot of differential conductance for Nb-InSb nanosheet hybrid device as a function of gate voltage  $V_g$  and magnetic field  $B$ , measured at  $T = 60$  mK. The typical Landau fan diagram with conductance plateaus of filling factor  $\nu = nh/eB = 1, 2, 3 \dots$  is observed. The dashed black lines track the same quantum Hall states in 2D InSb nanosheet. Left panel: resistance of the niobium electrodes as a function of magnetic field  $B$  at  $T = 60$  mK. The horizontal dashed line indicates the critical field of niobium ( $H_{c2} \sim 7$  T), below which an increase of conductance for the Nb-InSb nanosheet hybrid device is observed due to the superconducting proximity effect. (b) Gate-voltage dependence of differential conductance at different magnetic fields (2.7 T, 3.6 T, 6.3 T, 10.2 T). At  $B = 10.2$  T (blue trace) above  $H_{c2}$ , fully developed conductance plateaus are evident at  $\nu = 1, 3$ . Below  $H_{c2}$ , the conductance in the plateau region shows an enhancement, deviating from the expected quantized value.

### C. Quantum Hall effect in InSb nanosheets with Nb electrodes

The high upper critical field of Nb contacts ( $H_{c2} \sim 7$  T at 60 mK, see below), together with high electron mobility and the transparent interface of our hybrid devices, enable us to access the transport regime where the superconductivity and the quantum Hall effect in InSb nanosheets coexist. Here we perform the quantum Hall measurement with a two-terminal configuration, which has been used in small graphene samples to get rid of the effect of hot spots [46,47]. In the right panel of Fig. 3(a), the color-scaled differential conductance is plotted as a function of back-gate voltage and magnetic field for a Nb-InSb nanosheet device. As magnetic field  $B$  and the back-gate voltage  $V_g$  increase, a characteristic Landau fan diagram can be clearly discerned, indicating the development of the quantum Hall state in InSb nanosheets. The regions indicated by the black dashed lines correspond to plateaus in conductance, appearing as stripes fanning out from point  $B = 0$  and  $V_g = V_{th}$ . Landau-level formation is visible above  $B \sim 2$  T, demonstrating the high quality of our InSb nanosheet devices. With increasing  $B$ , a clear drop of conductance can be identified at the magnetic field 7 T, which appears as a sudden color change in the color map of conductance (more details can be seen in the Supplemental Material, Fig. S4 [38]). The left panel of Fig. 3(a) shows the resistance of a niobium test strip as a function of magnetic field  $B$  taken at 60 mK. The brown dashed line indicates the upper critical field of the niobium electrodes, where a drop of conductance in the hybrid device occurs. Below the critical field of Nb where the superconductivity and the quantum Hall state coexist, the increase of the conductance can be attributed to the Andreev reflection in the quantum Hall regime. In a weak disorder 2DEG-S interface, we can use an effective Landauer-Büttiker picture to depict the scattering at the interface. An electron edge state injects to the 2DEG-S interface from the quantum Hall edge and scatters into two Andreev-edge states at the corner with probabilities  $t_1$  and  $1 - t_1$ . The electron and hole mixed Andreev-edge states propagate along the interface until scattering themselves to either an electron or a hole edge state at the counter edge with probabilities  $t_2$  and  $1 - t_2$

[19,29]. Taking account of the electron-hole mixing in the edge channels, the total conductance can be expressed as  $G = 2G_0[t_1(1 - t_2) + t_2(1 - t_1)]$ , with  $G_0 = 2e^2/h$  [19,29]. For a transparent 2DEG-S interface, a number of edge channels participate in Andreev processes along the interface, resulting in enhanced conductance.

To further demonstrate the superconducting proximity effect on enhanced conductance at low magnetic fields, we show traces of  $G(V_g)$  at several representative fields in Fig. 3(b). Conductance traces in Fig. 3(b) show line cuts taken at the magnetic fields of 2.7, 3.6, 6.3, and 10.2 T, in which three are under and one is above the critical magnetic field of niobium contacts. The blue trace at  $B = 10.2$  T shows clear conductance plateaus that correspond to  $\nu = nh/eB = 1, 3$ , accompanied with conductance peaks indicated by black arrows. The other three conductance traces show similar peak features. This can be understood from the device geometry—two-terminal measurement of the quantum Hall effect is not straightforward. The measured conductance is always mixed with  $\sigma_{xx}$  and  $\sigma_{xy}$ , and the proportion of  $\sigma_{xx}$  in the component of the two-terminal conductance increases as the aspect ratio  $W/L$  increases [48]. As the aspect ratio  $W/L$  of the sample measured in Fig. 3 is about 30, the quantum Hall plateaus are mixed up with oscillations of  $\sigma_{xx}$ , as shown in Fig. 3(b). At  $B = 6.3$  T, which is near and below the critical magnetic field ( $H_{c2}$ ) of the niobium electrodes, the conductance in the plateau region starts to diverge from the expected quantized value. With decreasing the magnetic field, the vortices in the niobium film are sufficiently excluded. Therefore the Andreev-enhanced conductance at the plateau is more pronounced, which can be clearly seen in conductance traces measured at  $B = 2.7$  and 3.6 T. The increased conductance for the plateau is below the doubling of conductance relative to the normal state at 3.6 T, limited by the transparency of Nb-InSb nanosheet interfaces. Due to the proximity effect in the superconductor-normal metal-superconductor (SNS) structure, the increased conductance for the plateau at 2.7 T exceeds twice that derived from the Landau formula for a 2DEG-S interface discussed above.

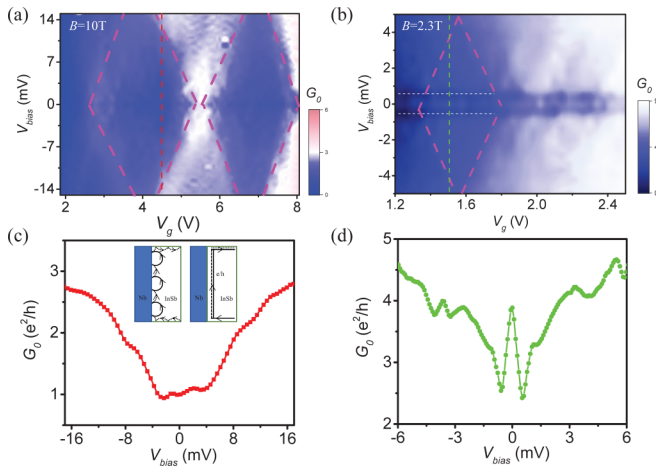


FIG. 4. Bias spectroscopy of Andreev reflection in the quantum Hall regime. (a), (b) Differential conductance  $G = dI_{sd}/dV_{bias}$  in units of  $e^2/h$  as a function of bias voltage and back-gate voltage, taken at 10 and 2.3 T, respectively. At  $B = 10$  T, the niobium contacts are driven into the normal state. The conductance map shows clear diamond-shaped structures highlighted by the magenta dashed lines, demonstrating the energy gap of Landau levels (LLs). At  $B = 2.3$  T, well below  $H_{c2}$ , the spectroscopy exhibits two symmetric ridges located around  $V_{bias} \simeq \pm 0.6$  mV (white dashed lines), corresponding to the superconducting gap of the Nb film for  $B = 2.3$  T. (c) Vertical line cut from (a) at the gate voltage indicated by the red dashed line. The conductance shows a suppression around zero bias, consistent with an opening gap between LLs. Inset: Schematic illustration demonstrating quasiclassical picture of an alternating electron-hole cyclotron motion due to Andreev reflection along the 2DEG-S interfaces (left) and coherent Andreev edge-state formation in the quantum Hall regime (right). (d) Vertical line cut from (b) at the gate voltage indicated by the green dashed line. It clearly displays a sharp zero-bias conductance peak when the Nb electrodes are superconducting.

#### D. Andreev reflection in the quantum Hall regime

We further investigate transport spectroscopy in the quantum Hall regime by performing the measurement of the differential conductance  $dI_{sd}/dV_{bias}$  as a function of  $V_g$  and the source-drain bias voltage  $V_{bias}$ . Figure 4(a) shows a 2D color plot of  $dI_{sd}/dV_{bias}$  versus both  $V_g$  and  $V_{bias}$  in the relevant quantum Hall regime, measured with  $B = 10$  T to suppress superconductivity. We see clearly a series of diamond-shaped regions indicated by the magenta dashed lines, where the differential conductance with  $V_{bias} \approx 0$  exhibits well-developed plateaus at the same gate voltages [Fig. 3(b)]. The light-blue regions correspond to low differential conductance. At each conductance plateau, the Fermi level lies between the Landau levels (LLs), and charge transport is dominated by the edge states, which are separated by an energy gap between LLs. As voltage bias is increased and aligned with the subsequent Landau level, the conductance increases rapidly (more details can be seen in the Supplemental Material, Fig. S5 [38]). As shown in Fig. 4(a), bias spectroscopy measurements show diamond-shaped light-blue regions in which the differential conductance is suppressed as a result of the energy gap of LLs. The above spectroscopy behavior is qualitatively very similar to that of one-dimensional subbands in ballistic quantum

point contacts [15]. From the height of diamond, we can estimate the energy scale for the Landau-level energy spacing in InSb nanosheet, which is of the order of 23 meV for the first filling factor at  $B = 10$  T. We also explore the evolution of bias spectroscopy on magnetic field (see Fig. S6 in the Supplemental Material [38]). The size of the diamond-shaped regions for the same filling factor, providing a measure of the energy gap of Landau levels, agrees with the expected linear dependence on magnetic field.

We further examine the bias spectroscopy in the regime with the coexistence of superconductivity and the quantum Hall states. In Fig. 4(b), we present a plot of the measured differential conductance of the same device as a function of  $V_g$  and  $V_{bias}$ , taken at  $B = 2.3$  T, which is well below the critical field of Nb film. The diamond-shaped structures can be also resolved in the 2D plot, denoting the formation of LLs. While taking a further look at a low-bias regime, the spectroscopy exhibits two symmetric ridges located at  $V_{bias} \simeq \pm 0.6$  mV, being independent of gate voltage. Its position corresponds approximately to the value of the superconducting gap of the Nb film for  $B = 2.3$  T, estimated from BCS theory with the measured zero-field superconducting energy gap. Taken together, the bias-dependent transport measurement provides a spectroscopic evidence of the coexistence of the Landau level and proximity-induced superconductivity in our InSb nanosheet hybrid devices.

The most noticeable feature is that there are two different subgap structures appearing around  $V_{bias} \approx 0$  V, obtained in the quantum Hall regime with and without superconductivity. In Figs. 4(c) and 4(d), we show typical  $dI_{sd}/dV_{bias}$ -versus- $V_{bias}$  traces taken within the diamond-shaped regions, as indicated by the dashed lines in Figs. 4(a) and 4(b). At  $B = 10$  T, the  $dI_{sd}/dV_{bias}$  displays a suppression of conductance around zero bias, consistent with an opening gap between LLs as discussed above [see Fig. 4(c)]. In contrast, in the low-magnetic-field coexisting region of quantum Hall states and superconductivity, we observe that the  $dI/dV$  exhibits a pronounced peak at around zero bias [see Fig. 4(d)]. For a transparent interface, the Andreev reflection process is manifested by an enhancement of the subgap conductance, which has been reported before in various superconductor-normal conductor hybrid devices [49–53]. The height of zero-bias conductance peak is dependent on the Andreev reflection probability at the interface [49,50]. Therefore, the observed zero-bias conductance peak is directly related to the Andreev reflection occurring at the superconductor-InSb interface in the quantum Hall regime. In the picture of the conventional phase-coherent Andreev reflection, the enhanced subgap conductance can be strongly suppressed by a small magnetic field, inconsistent with our experimental results.

We now discuss that the observed zero-bias conductance peak at high fields can be understood in terms of the formation of Andreev edge states in the quantum Hall regime [26]. At a 2DEG-superconductor (2DEG-S) interface, a strong magnetic field forces the charge carriers into chiral edge channels, and the Andreev reflection process is quite different from that at zero magnetic field. An electron hitting the interface performs an Andreev reflection, forming a Cooper pair in the superconductor and retroreflecting a hole into the 2DEG. The retroreflected hole lives in the same band with the impinging

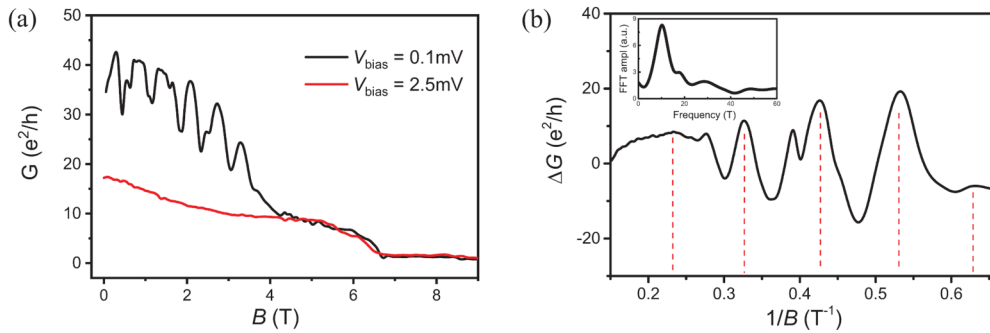


FIG. 5. Pronounced magnetoconductance oscillations in Nb-InSb nanosheet hybrid devices. (a) Magnetoconductance at  $V_{\text{bias}} = 0.1$  mV (subgap) and  $V_{\text{bias}} = 2.5$  mV (above gap). The subgap conductance clearly exhibits a pronounced oscillations under 4 T relative to above-gap conductance. (b) Conductance oscillation  $\Delta G_s$  as a function of inverse magnetic field  $1/B$ . Vertical dashed line indicates equal periods of oscillations. The inset shows the Fourier transform of the oscillations, which exhibits a single peak.

electron. In a quasiclassical picture, it forms an alternating electron-hole cyclotron motion along the 2DEG-S interface since electron-hole conversion changes the sign of the effective mass and Lorentz force under applied magnetic fields, as shown in the inset of Fig. 4(c). Theoretical studies have suggested that a novel kind of Andreev bound state can be formed at the 2DEG-S interface. This bound state is a coherent superposition of electrons and holes propagating in the same direction along the 2DEG-S interface [Fig. 4(c), inset], forming the so-called Andreev edge states [26,54–56]. Such a process gives rise to a high cumulative Andreev reflection probability, resulting in a pronounced peak around zero bias in the quantum Hall regime.

To further investigate the impact of Andreev reflection on transport in high magnetic fields, we perform magnetoconductance measurements on hybrid devices at fixed gate voltage. In Fig. 5(a), we show the measured subgap conductance (black line) and above-gap conductance (red line) traces of device D2 as a function of magnetic field for  $V_g = 3.8$  V, respectively. The above-gap differential conductance  $G_n$  is taken at high bias voltage ( $V_{\text{bias}} = 2.5$  mV) above the superconducting gap of Nb, corresponding to the normal state conductance. The subgap conductance  $G_s$  is taken at  $V_{\text{bias}} = 0.1$  mV within the superconducting gap. Below the critical field of Nb, the above-gap conductance is significantly suppressed compared to the subgap conductance due to the proximity effect. A more interesting phenomenon is that the subgap conductance exhibits a pronounced magnetoconductance oscillations before the destruction of superconductivity in Nb electrode. With further increasing magnetic field, the conductance oscillation disappears with further developing into quantum Hall plateaus. For further analyzing the oscillatory part of subgap conductance, we plot  $\Delta G_s$  as a function of inverse magnetic field after subtracting the smooth polynomial background. As shown in Fig. 5(b), the  $\Delta G_s$  exhibits periodic oscillation in  $1/B$ , which is the characteristic behavior of the Shubnikov–de Haas (SdH) oscillation. By taking the Fourier transform of the oscillations, a single frequency can be clearly identified, as shown in the inset of Fig. 5(b). A similar behavior of enhanced SdH oscillations has been observed in previous experiments on InAs-based hybrid devices with niobium stripe arrays [57]. For an interface with weak disorder and a small Fermi wavelength mismatch, enhanced conductance oscillations as

a function of magnetic field have been theoretically predicted to originate from the transmission resonance through Andreev edge states [26,54–56]. An interference between normal and Andreev reflections gives rise to  $1/B$ -periodic SdH-like oscillations [26,54,57]. It is therefore suggested that the observed enhancement of SdH oscillations in our hybrid devices is a manifestation of Andreev edge states propagating along the superconductor-InSb nanosheet interface in the quantum Hall regime.

#### IV. CONCLUSION

In conclusion, we have presented the realization and transport characterization of hybrid superconducting devices based on two-dimensional single-crystalline InSb nanosheets. The hybrid devices exhibit gate-tunable superconducting proximity effect and multiple Andreev reflections, indicating that transparent interfaces between superconducting electrodes and nanosheets are obtained. Below the critical field of superconducting Nb electrodes, we demonstrate the coexistence of proximity-induced superconductivity and quantum Hall states in hybrid InSb nanosheet devices, as evidenced by the Landau fan diagram and transport spectroscopy measurements. In these coexisting regions, we observed an enhancement of conductance at the quantum Hall plateaus, accompanied by a pronounced zero-bias peak in differential conductance. The observed behavior is consistent with the formation of Andreev edge states propagating along the superconductor-InSb nanosheet interface in the quantum Hall regime. These results are an important advance toward building scalable topological superconducting devices based on 2D semiconducting nanosheets with strong spin-orbit coupling.

#### ACKNOWLEDGMENTS

We acknowledge financial support from the National Key Research and Development Program of China (Grants No. 2016YFA0300601 and No. 2017YFA0303304), the National Natural Science Foundation of China (Grants No. 11774005, No. 11874071, No. 91221202, and No. 91421303), and the Beijing Academy of Quantum Information Sciences (Grant No. Y18G22).

- [1] J. A. Del Alamo, Nanometre-scale electronics with III–V compound semiconductors, *Nature (London)* **479**, 317 (2011).
- [2] R. Chau, B. Doyle, S. Datta, J. Kavalieros, and K. Zhang, Integrated nanoelectronics for the future, *Nat. Mater.* **6**, 810 (2007).
- [3] H. Ko, K. Takei, R. Kapadia, S. Chuang, H. Fang, P. W. Leu, K. Ganapathi, E. Plis, H. S. Kim, S.-Y. Chen *et al.*, Ultrathin compound semiconductor on insulator layers for high-performance nanoscale transistors, *Nature (London)* **468**, 286 (2010).
- [4] J. Orr, A. Gilbertson, M. Fearn, O. Croad, C. Storey, L. Buckle, M. Emeny, P. Buckle, and T. Ashley, Electronic transport in modulation-doped InSb quantum well heterostructures, *Phys. Rev. B* **77**, 165334 (2008).
- [5] V. Pribiag, S. Nadj-Perge, S. M. Frolov, J. Van Den Berg, I. Van Weperen, S. Plissard, E. Bakkers, and L. P. Kouwenhoven, Electrical control of single hole spins in nanowire quantum dots, *Nat. Nanotechnol.* **8**, 170 (2013).
- [6] S. Nadj-Perge, V. Pribiag, J. Van den Berg, K. Zuo, S. Plissard, E. Bakkers, S. M. Frolov, and L. P. Kouwenhoven, Spectroscopy of Spin-Orbit Quantum Bits in Indium Antimonide Nanowires, *Phys. Rev. Lett.* **108**, 166801 (2012).
- [7] D. Fan, S. Li, N. Kang, P. Caroff, L. Wang, Y. Huang, M. Deng, C. Yu, and H. Xu, Formation of long single quantum dots in high quality InSb nanowires grown by molecular beam epitaxy, *Nanoscale* **7**, 14822 (2015).
- [8] R. M. Lutchyn, J. D. Sau, and S. D. Sarma, Majorana Fermions and a Topological Phase Transition in Semiconductor-Superconductor Heterostructures, *Phys. Rev. Lett.* **105**, 077001 (2010).
- [9] Y. Oreg, G. Refael, and F. von Oppen, Helical Liquids and Majorana Bound States in Quantum Wires, *Phys. Rev. Lett.* **105**, 177002 (2010).
- [10] V. Mourik, K. Zuo, S. M. Frolov, S. Plissard, E. P. Bakkers, and L. P. Kouwenhoven, Signatures of Majorana fermions in hybrid superconductor-semiconductor nanowire devices, *Science* **336**, 1003 (2012).
- [11] M. Deng, C. Yu, G. Huang, M. Larsson, P. Caroff, and H. Xu, Anomalous zero-bias conductance peak in a Nb–InSb nanowire–Nb hybrid device, *Nano Lett.* **12**, 6414 (2012).
- [12] H. Zhang, Ö. Gül, S. Conesa-Boj, M. P. Nowak, M. Wimmer, K. Zuo, V. Mourik, F. K. de Vries, J. van Veen, M. W. de Moor *et al.*, Ballistic superconductivity in semiconductor nanowires *Nat. Commun.* **8**, 16025 (2017).
- [13] Ö. Gül, H. Zhang, J. D. Bommer, M. W. de Moor, D. Car, S. R. Plissard, E. P. Bakkers, A. Geresdi, K. Watanabe, T. Taniguchi *et al.*, Ballistic Majorana nanowire devices, *Nat. Nanotechnol.* **13**, 192 (2018).
- [14] M. Hell, K. Flensberg, and M. Leijnse, Coupling and braiding Majorana bound states in networks defined in two-dimensional electron gases with proximity-induced superconductivity, *Phys. Rev. B* **96**, 035444 (2017).
- [15] F. Qu, J. van Veen, F. K. de Vries, A. J. Beukman, M. Wimmer, W. Yi, A. A. Kiselev, B.-M. Nguyen, M. Sokolich, M. J. Manfra *et al.*, Quantized conductance and large g-factor anisotropy in InSb quantum point contacts, *Nano Lett.* **16**, 7509 (2016).
- [16] T. D. Stanescu and S. D. Sarma, Building topological quantum circuits: Majorana nanowire junctions, *Phys. Rev. B* **97**, 045410 (2018).
- [17] M. Kjaergaard, F. Nichele, H. J. Suominen, M. P. Nowak, M. Wimmer, A. R. Akhmerov, J. A. Folk, K. Flensberg, J. Shabani, C. J. Palmstrom, and C. M. Marcus, Quantized conductance doubling and hard gap in a two-dimensional semiconductor-superconductor heterostructure, *Nat. Commun.* **7**, 12841 (2016).
- [18] F. Amet, C. T. Ke, I. V. Borzenets, J. Wang, K. Watanabe, T. Taniguchi, R. S. Deacon, M. Yamamoto, Y. Bomze, S. Tarucha *et al.*, Supercurrent in the quantum Hall regime, *Science* **352**, 966 (2016).
- [19] P. Rickhaus, M. Weiss, L. Marot, and C. Schönenberger, Quantum Hall effect in graphene with superconducting electrodes, *Nano Lett.* **12**, 1942 (2012).
- [20] G.-H. Lee, K.-F. Huang, D. K. Efetov, D. S. Wei, S. Hart, T. Taniguchi, K. Watanabe, A. Yacoby, and P. Kim, Inducing superconducting correlation in quantum Hall edge states., *Nat. Phys.* **13**, 693 (2017).
- [21] N. H. Lindner, E. Berg, G. Refael, and A. Stern, Fractionalizing Majorana Fermions: Non-Abelian Statistics on the Edges of Abelian Quantum Hall States, *Phys. Rev. X* **2**, 041002 (2012).
- [22] D. J. Clarke, J. Alicea, and K. Shtengel, Exotic non-Abelian anyons from conventional fractional quantum Hall states, *Nat. Commun.* **4**, 1348 (2013).
- [23] R. S. Mong, D. J. Clarke, J. Alicea, N. H. Lindner, P. Fendley, C. Nayak, Y. Oreg, A. Stern, E. Berg, K. Shtengel *et al.*, Universal Topological Quantum Computation from a Superconductor-Abelian Quantum Hall Heterostructure, *Phys. Rev. X* **4**, 011036 (2014).
- [24] P. San-Jose, J. L. Lado, R. Aguado, F. Guinea, and J. Fernández-Rossier, Majorana Zero Modes in Graphene, *Phys. Rev. X* **5**, 041042 (2015).
- [25] Z. Wan, A. Kazakov, M. J. Manfra, L. N. Pfeiffer, K. W. West, and L. P. Rokhinson, Induced superconductivity in high-mobility two-dimensional electron gas in gallium arsenide heterostructures, *Nat. Commun.* **6**, 7426 (2015).
- [26] H. Hoppe, U. Zülicke, and G. Schön, Andreev Reflection in Strong Magnetic Fields, *Phys. Rev. Lett.* **84**, 1804 (2000).
- [27] F. Giazotto, M. Governale, U. Zülicke, and F. Beltram, Andreev reflection and cyclotron motion at superconductor - normal-metal interfaces, *Phys. Rev. B* **72**, 054518 (2005).
- [28] Y. Takagaki, Transport properties of semiconductor-superconductor junctions in quantizing magnetic fields, *Phys. Rev. B* **57**, 4009 (1998).
- [29] I. Khaymovich, N. Chtchelkatchev, I. Shereshevskii, and A. Mel'nikov, Andreev transport in two-dimensional normal-superconducting systems in strong magnetic fields, *EPL* **91**, 17005 (2010).
- [30] N. M. Chtchelkatchev and I. S. Burmistrov, Conductance oscillations with magnetic field of a two-dimensional electron gas–superconductor junction, *Phys. Rev. B* **75**, 214510 (2007).
- [31] T. D. Moore and D. Williams, Andreev reflection at high magnetic fields, *Phys. Rev. B* **59**, 7308 (1999).
- [32] G. H. Park, M. Kim, K. Watanabe, T. Taniguchi, and H. J. Lee, Propagation of superconducting coherence via chiral quantum-Hall edge channels, *Sci. Rep.* **7**, 10953 (2017).
- [33] D. J. Clarke, J. Alicea, and K. Shtengel, Exotic circuit elements from zero-modes in hybrid superconductor–quantum-Hall systems, *Nat. Phys.* **10**, 877 (2014).

- [34] Z. Hou, Y. Xing, A.-M. Guo, and Q.-F. Sun, Crossed Andreev effects in two-dimensional quantum Hall systems, *Phys. Rev. B* **94**, 064516 (2016).
- [35] D. Pan, D. Fan, N. Kang, J. Zhi, X. Yu, H. Xu, and J. Zhao, Free-standing two-dimensional single-crystalline InSb nanosheets, *Nano Lett.* **16**, 834 (2016).
- [36] W. Yi, A. A. Kiselev, J. Thorp, R. Noah, B.-M. Nguyen, S. Bui, R. D. Rajavel, T. Hussain, M. F. Gyure, P. Kratz, Q. Qian, M. J. Manfra, V. S. Pribiag, L. P. Kouwenhoven, C. M. Marcus, and M. Sokolich, Gate-tunable high mobility remote-doped InSb/In<sub>1-x</sub>Al<sub>x</sub>Sb quantum well heterostructures, *Appl. Phys. Lett.* **106**, 142103 (2015).
- [37] M. M. Uddin, H. W. Liu, K. F. Yang, K. Nagase, T. D. Mishima, M. B. Santos, and Y. Hirayama, Characterization of InSb quantum wells with atomic layer deposited gate dielectrics, *Appl. Phys. Lett.* **101**, 233503 (2012).
- [38] See Supplemental Material at <http://link.aps.org/supplemental/10.1103/PhysRevB.99.245302> for more detailed nanosheet growth, device description, as well as additional analysis and measurements, which include Refs. [39–41].
- [39] W. Mayer, J. Yuan, K. S. Wickramasinghe, T. Nguyen, M. C. Dartiailh, and J. Shabani, Superconducting proximity effect in epitaxial Al-InAs heterostructures, *Appl. Phys. Lett.* **114**, 103104 (2019).
- [40] R. J. Nicholas, R. J. Haug, K. v. Klitzing, and G. Weimann, Exchange enhancement of the spin splitting in a GaAs – Ga<sub>x</sub>Al<sub>1-x</sub>As heterojunction, *Phys. Rev. B* **37**, 1294 (1988).
- [41] J. Velasco, Jr., Y. Lee, Z. Zhao, L. Jing, P. Kratz, M. Bockrath, and C. N. Lau, Transport measurement of Landau level gaps in bilayer graphene with layer polarization control, *Nano Lett.* **14**, 1324 (2014).
- [42] K. Flensberg, J. B. Hansen, and M. Octavio, Subharmonic energy-gap structure in superconducting weak links, *Phys. Rev. B* **38**, 8707 (1988).
- [43] M. Octavio, M. Tinkham, G. Blonder, and T. Klapwijk, Subharmonic energy-gap structure in superconducting constrictions, *Phys. Rev. B* **27**, 6739 (1983).
- [44] Y. J. Doh, J. A. van Dam, A. L. Roest, E. P. Bakkers, L. P. Kouwenhoven, and S. De Franceschi, Tunable supercurrent through semiconductor nanowires, *Science* **309**, 272 (2005).
- [45] J. Xiang, A. Vidan, M. Tinkham, R. M. Westervelt, and C. M. Lieber, Ge/Si nanowire mesoscopic Josephson junctions, *Nat. Nanotechnol.* **1**, 208 (2006).
- [46] I. Skachko, X. Du, F. Duerr, A. Luican, D. A. Abanin, L. S. Levitov, and E. Y. Andrei, Fractional quantum Hall effect in suspended graphene probed with two-terminal measurements, *Philos. Trans. R. Soc. London, Ser. A* **368**, 5403 (2010).
- [47] X. Du, I. Skachko, F. Duerr, A. Luican, and E. Y. Andrei, Fractional quantum Hall effect and insulating phase of Dirac electrons in graphene, *Nature (London)* **462**, 192 (2009).
- [48] D. A. Abanin and L. S. Levitov, Conformal invariance and shape-dependent conductance of graphene samples, *Phys. Rev. B* **78**, 035416 (2008).
- [49] G. Blonder, M. Tinkham, and T. Klapwijk, Transition from metallic to tunneling regimes in superconducting microconstrictions: Excess current, charge imbalance, and supercurrent conversion, *Phys. Rev. B* **25**, 4515 (1982).
- [50] B. Van Wees, P. De Vries, P. Magnée, and T. Klapwijk, Excess Conductance of Superconductor-Semiconductor Interfaces due to Phase Conjugation Between Electrons and Holes, *Phys. Rev. Lett.* **69**, 510 (1992).
- [51] P. Xiong, G. Xiao, and R. Laibowitz, Subgap and Above-Gap Differential Resistance Anomalies in Superconductor-Normal-Metal Microjunctions, *Phys. Rev. Lett.* **71**, 1907 (1993).
- [52] Z. Kvon, T. Baturina, R. Donaton, M. Baklanov, K. Maex, E. Olshanetsky, A. Plotnikov, and J. Portal, Proximity effects and Andreev reflection in a mesoscopic SNS junction with perfect NS interfaces, *Phys. Rev. B* **61**, 11340 (2000).
- [53] F. Yang, Y. Ding, F. Qu, J. Shen, J. Chen, Z. Wei, Z. Ji, G. Liu, J. Fan, C. Yang *et al.*, Proximity effect at superconducting Sn – Bi<sub>2</sub>Se<sub>3</sub> interface, *Phys. Rev. B* **85**, 104508 (2012).
- [54] Y. Asano, Magnetoconductance oscillations in ballistic semiconductor-superconductor junctions, *Phys. Rev. B* **61**, 1732 (2000).
- [55] N. Chtchelkatchev, Conductance of a semiconductor (2DEG)-superconductor junction in high magnetic field, *J. Exp. Theor. Phys. Lett.* **73**, 94 (2001).
- [56] M. Ma and A. Y. Zyuzin, Josephson effect in the quantum Hall regime, *EPL* **21**, 941 (1993).
- [57] J. Eroms, D. Weiss, J. De Boeck, G. Borghs, and U. Zülicke, Andreev Reflection at High Magnetic Fields: Evidence for Electron and Hole Transport in Edge States, *Phys. Rev. Lett.* **95**, 107001 (2005).